

Production of ring-like structure in the cocoon of Hercules A

Curtis J. Saxton^{1,2}

and

Geoffrey V. Bicknell^{2,1}

and

Ralph S. Sutherland²

ABSTRACT

The radio lobes of the radio galaxy Hercules A contain intriguing ring-like structures concentric with the jet axis. To investigate the occurrence of such features, we have used hydrodynamic simulations of jets with a range of Mach numbers (from $M = 2$ to 50) and densities (down to a ratio of 10^{-4} relative to the background) to generate ray-traced images simulating synchrotron emission from the time-dependent shock structures. We compare these images with observations of Hercules A, and consider the physical nature and temporal evolution of the most plausible configurations. We find that the observed ring-like structures are well explained as nearly annular shocks propagating in the backflow surrounding the jet. We infer that the jet is oriented at between 30° and 70° to the line of sight, consistent with radio depolarisation observations of Gizani & Leahy. The observational lack of hot-spots at the extremities of the radio lobes, and the possible presence of a buried hot-spot near the base of the western lobe, are explained in terms of the intrinsic brightness fluctuations and dynamics of the terminal shock of an ultra-light, low Mach number jet that surges along its axis due to intermittent pinching and obstruction by turbulent backflow in the cocoon. We conclude from the appearance of both sides of the Hercules A, that both jets are on the borderline of becoming fully turbulent.

Subject headings: hydrodynamics — galaxies: active — galaxies: individual (Hercules A; 3C 348) — galaxies: jets — radio continuum: galaxies — X-rays: galaxies

¹Department of Physics & Theoretical Physics, Faculty of Science, Australian National University, ACT 0200, Australia

²Research School of Astronomy & Astrophysics, Mt Stromlo Observatory, Australian National University, Cotter Road, Weston ACT 2611, Australia

1. Introduction

Hercules A (3C 348) is a luminous radio galaxy (Dreher & Feigelson 1984; Mason et al. 1988) at a redshift of $z = 0.154$, in a cluster of uncertain richness (Greenstein 1962; Owen & Laing 1989; Yates et al. 1989; Allington-Smith et al. 1993). Its total power at 5 GHz, $P_{5\text{GHz}} \approx 4.9 \times 10^{25}/h^2 \text{ W Hz}^{-1}$, if $H_0 = 70h \text{ km s}^{-1} \text{ Mpc}^{-1}$ (Gizani & Leahy 1999). In optical observations, the elliptical galaxy is found to have a double nucleus (with a separation $\sim 4''$) and tail-like distortions of the stellar isophotes implying a merger of galaxies (Minkowski 1957; Sadun & Hayes 1993).

The X-ray emitting cluster medium was the subject of ASCA and ROSAT observations by Siebert et al. (1999) and ROSAT observations by Gizani & Leahy (1999). The diffuse X-ray distribution is elongated in the direction of the radio source axis, suggesting an interaction with the radio lobes. The medium is otherwise well described by a β -model profile with best-fit parameters $\beta \approx 0.63$ and core radius $r_c \approx 35 \pm 3''$ (Siebert et al. 1999). The contribution from the nucleus is $\lesssim 3\%$ of total X-ray luminosity, but the cluster surface brightness may be centrally peaked (Gizani & Leahy 1999). However there may actually be two thermal X-ray emitting components present, as the ASCA spectrum suggests a temperature $kT \approx 4.3\text{keV}$ and a central electron density of $n_0 \approx 9.1 \times 10^{-3} \text{ cm}^{-3}$, whereas the ROSAT/PSPC spectrum suggests $kT \approx 2.4\text{keV}$. ROSAT observations by Gizani et al. (2002) determined a temperature $kT = 2.45 \text{ keV}$ and $n_0 = 7.8 \times 10^{-3} \text{ cm}^{-3}$. Trussoni et al. (2001) presented BeppoSAX observations indicating a temperature 4–5 keV with the possibility of an additional $\sim 3 \text{ keV}$ component.

In VLA observations, Gizani & Leahy (1999) found that the cluster medium affects the depolarisation of the radio features: the western side exhibits greater depolarisation than the east. As the more distant jet and lobe are seen through a thicker column of the cluster medium, they deduced a jet inclination of $\theta \approx 50^\circ$ to the line of sight. Thus Hercules A exhibits a classical Laing-Garrington effect (Laing 1988; Garrington et al. 1988).

The radio lobes span $\sim 3'$ and in overall shape they are symmetric about the nucleus (see Figure 1), although the eastern lobe accounts for 3/4 of the total radio luminosity. Although the radio power of Hercules A is in the range of FR2 sources (See Fanaroff & Riley 1974) the morphology of the radio lobes belongs ambiguously to the FR1 class. Most notably, neither lobe shows a hot-spot near its outer extremity.

The western radio lobe (on side of the receding jet) contains a sequence of arc-like and ring-like features that are brighter than the lobe, and which are approximately concentric with the jet axis (Dreher & Feigelson 1984; Mason et al. 1988). The most distinct of these features, and the furthest from the nucleus, is a “semi-ring” that is bright on only one

side. Radio emission from the rings is linearly polarised: up to $\sim 50\%$ in the two outer rings (Dreher & Feigelson 1984). The radio spectral indices are flatter in the jets and rings ($\alpha \approx 1.1$ where $S_\nu \propto \nu^{-\alpha}$) than in the radio lobes generally ($\alpha \approx 1.6$), indicating that the radio emitting plasma in the rings is younger than the background (Gizani & Leahy 1999; Gizani et al. 2002). The eastern (approaching) jet shows “helical” features, which may be a projected superposition of rings (Gizani et al. 2002).

The radio lobes of some other galaxies display ring-like internal structures, which have been likened to the rings in the western lobe of Hercules A (Morrison & Sadun 1996). The source 3C 310 also shows several circular features in both the northern and southern lobes; these rings are larger in proportion to the lobes than those of Hercules A (van Breugel & Fomalont 1984; Morrison & Sadun 1996). Other radio galaxies with ring-like features include MG 0248 + 0641 (Conner et al. 1998) and 3C 219 (Perley et al. 1980).

Several explanations have been offered for the nature and origin of the rings. Dreher & Feigelson (1984) suggested that the rings in Hercules A originate as distinct ejections from the nucleus, or interruptions of the jet due to either intrinsic pinching instabilities or collisions with clouds straying into the jet axis. In that case, the bright rings are surfaces where the ambient radio lobe or cluster medium contacts and interacts with a cloud.

Mason et al. (1988) proposed that the jet loses collimation at the point where the radio structure widens, and that concentrated streams of relativistic protons intermittently cross or self-cross, causing energetic particle bursts which deposit kinetic energy in the plasma at that site. These disturbances expand spherically, as they drift outwardly within the medium of the radio lobe. In this scenario, the rings are the projected edges of the spheres. This would account for the approximately linear relation between ring radius and displacement from the core.

Morrison & Sadun (1996) proposed a qualitatively similar theory in which uniformly expanding spheres originate as acoustic disturbances carried outwardly in a galactic wind. The subsequent onset of jet activity then floods the region with radio-emitting material. Radio-bright plasma interacts with the shells and tends to concentrate on the surfaces of these structures. One implication of this model is that the extensive wind has an age of Gigayears. However in our view this requirement may be difficult to reconcile with the likely disturbances in the cluster environment of Hercules A, especially related to the merger of another galaxy with Hercules A (as implied by the double nucleus and stellar tail, Sadun & Hayes 1993). Thus we are motivated to consider an alternative model in which the formation of rings is intrinsic to jet and lobe dynamics.

In Saxton et al. (2002) we simulated the interactions of a hypersonic, low mass jet

within its turbulent cocoon, covering a parameter-space with two orders of magnitude in jet density and Mach numbers from 5 to 50. We considered the dynamics of point-like and ring-like shocks near the head of the jet, in order to model and interpret the complex shock structures observed near the western hot-spot of Pictor A. In the present paper, we use the database of adiabatic jet simulations of Saxton et al. (2002), augmented by some additional simulations, to generate synthetic radio maps resembling the morphology and brightness distribution of the features of Hercules A. We propose a model of the radio rings as annular shocks propagating in the cocoon backflow in the western radio lobe.

2. Simulations

Our hydrodynamic simulations were conducted using the Piecewise Parabolic Method (PPM) (Colella & Woodward 1984) implemented in a code based on the VH-1 code (Blondin & Lukfin 1993). An advantage of PPM for this type of simulation is its excellent shock-capturing properties. We have enhanced the code to achieve greater efficiency, and have added a scalar tracer variable φ that is passively advected with the flow. By assigning $\varphi = 1$ within jet plasma entering the grid, and initially $\varphi = 0$ in the background medium, we use this variable to distinguish and follow the evolution of the constituents of the physical system.

Our images of simulated radio surface brightness were rendered by a ray-tracing program that projects three-dimensional structures obtained from the PPM output. Assuming that the magnetic pressure is approximately proportional to the hydrodynamic pressure, p , the volumetric emissivity, $j_\nu \propto \varphi p^{(3+\alpha)/2}$. This ansatz is only valid at a frequency that is less than any cooling-induced break in frequency so that to be consistent we choose a value of $\alpha = 0.6$. This is flatter than the observed spectral index in, for example, the rings wherein $\alpha = 1.1$ (Gizani et al. 2002) indicating that these features are older than the synchrotron cooling time. Our assumption of $\alpha = 0.6$ means that the relative contrast of features will be affected. However, the resulting images obtained by integrating j_ν along given lines of sight for each pixel of the simulated intensity map, should give a good qualitative indication of the appearance of the flow and also give a good indication of the relative contrast of features as a function of jet parameters. (This is an important point that is discussed below in § 4.2

Despite the importance of synchrotron and/or inverse Compton cooling for the radio spectrum, cooling does not affect the hydrodynamics of the flow since the lowest energy particles that dominate the internal energy are unaffected. Therefore, the way the system behaves depends on dimensionless parameters such as the density ratio of jet to ambient gas, η , the corresponding pressure ratio (assumed equal to one), and the Mach number of the jet,

$M \equiv v_j/c_{s,\text{igm}}$. Our simulations cover a parameter space defined by $\eta = 10^{-2}, 10^{-3}, 10^{-4}$ and $M = 2, 5, 10, 50$. Adopting the cooler estimate of the temperature and density in the ambient cluster medium as fiducial scales for our simulations, the thrust and power of the simulated jets are given in Table 1. These are classical values, and can be related to parameters of relativistic jets with equivalent thrust or power (e.g. Rosen et al. 1999; Carvalho & O’Dea 2001). Using the parameter κ_ν , which is the ratio of monochromatic radio lobe power at frequency ν to jet luminosity, we have for values of $\kappa_{1.4} \sim 10^{-11} - 10^{-12} \text{ Hz}^{-1}$ (see Bicknell et al. 1998) and total flux density $\approx 48 \text{ Jy}$, a jet luminosity $\sim 10^{45-46} \text{ erg s}^{-1}$ and a thrust $\sim 4 \times 10^{34-35} \text{ dyn}$. The time interval between output frames of the hydrodynamic data was set so that approximately 600 frames were generated before the jet reached the right side (large z) boundary of the grid.

We assume that the outer boundaries of the computational grid are open to outflow, except at the base of the jet at the left (low- z) boundary. The initial properties of the jet are copied to those cells at the start of each time step, in order to maintain a jet with constant mass flux, thrust and power. In Saxton et al. (2002) we concentrated on cases in which a reflecting condition applies at the left boundary, representing effects near the plane of symmetry near the nucleus producing equally strong, opposite jets. The closed boundary condition was found to lead to a conical cocoon which is typically much wider than the cylindrical cocoons that develop about jets in simulations with an open left boundary. The latter represent the effects of systems where the head of the jet is causally distant from the nucleus and the plane of symmetry about the galaxy. We will initially focus our discussion on simulations with this type of boundary condition, as this seems physically appropriate for Hercules A, since the radio lobes extend hundreds of kiloparsecs from the galaxy.

As seen in the radio intensity maps of Dreher & Feigelson (1984), the jet diameter is $\lesssim 0.5''$, the resolution of the image, corresponding to a radius $r_j \approx 0.54/h \text{ kpc}$ if $H_0 = 70h \text{ km s}^{-1} \text{ Mpc}^{-1}$ implying a scale $1'' = 2.4/h \text{ kpc}$. This scale is assumed in Table 1.

3. Results

The morphology of our simulated brightness maps is determined by the distribution of bright shock features. The termination shock of the jet is often, but not always, the brightest of such features. Biconical (“diamond”) shocks also occur within the jet, caused by disturbances from turbulence in the surrounding cocoon. Transient annular shocks also occur in the inner parts of the jet backflow; these features are particularly frequent near the head of the jet.

In Saxton et al. (2002) it was shown that jets rendered at orientations almost in the plane of the sky, $70^\circ \lesssim \theta \lesssim 90^\circ$, may show round hot-spots and knots on the jet axis, plus more spatially extended and transient shock features that appear almost linear in projection. These do not resemble the arcs of Hercules A. Neither do we find morphologies resembling Hercules A when jets are rendered at a small angle to the line of sight, $\theta \lesssim 30^\circ$: in such cases the extended shock features appear in projection as a clutter of tightly overlapping circles and knots. We find the best resemblance in frames rendered at $\theta \approx 45^\circ$. Examples from simulations with a range of jet parameters (η, M) are shown in Figures 4-11.

As detailed in Saxton et al. (2002), the hot-spot vanishes and reforms in an irregular cycle in which the jet is pinched off and temporarily obstructed by turbulence and/or the entrainment of dense gas in the cocoon, followed by the jet burrowing forward again. The effect of turbulence was documented in Saxton et al. (2002). This surging is most extensive and frequent for jets with low η . In the present paper, we also show in Figure 3, the effect of the latter mechanism. Dense gas is entrained into the cocoon and directly impedes the jet. This effect is particularly prominent at low Mach numbers, as one would expect. In the density images in the figure we show a time series of snapshots that show dense (white) fingers of gas entrained into the lobe and partially, then totally, obstructing the passage of an $(\eta, M) = (10^{-4}, 2)$ jet. For a time, the extreme end of the lobe is being starved of jet plasma and consequently does not show a hot-spot.

In a significant fraction of instants in each of our simulations of light jets, the hot-spot is temporarily absent or dimmer than one or more brighter shock structures in the backflow, such as annular rings. This occurs approximately 20%–50% of the time at all Mach numbers. To quantify the location of the hot-spot, we show in Figure 2 the trends in the cumulative distributions of the ratios of the hot-spot to bow shock locations. That is, the plots show the probability that the ratio of hot-spot distance to bow-shock distance is less than a certain value. Note that the probability of a embedded hot-spot is greater at $M = 2$ and also, for a given Mach number, at lower η .

Let us discuss some of the features of the simulations and in particular their dependence on Mach number and density ratio. The jet Mach number has a substantial effect on the typical brightness contrast between the background radio lobe and the shock features near the head of the jet. As expected in principle, and as shown in our previous studies (Saxton et al. 2002), for a given value of η the cases with a larger jet Mach number show a greater brightness contrast. As M increases, the ray-traced intensity maps are increasingly dominated by the transient frontal shock features near the head of the jet: a bright hot-spot comprising the jet termination shock, one of the nearer biconical shocks within the jet, or else a singularly bright annular shock emerging from the division of an older hot-spot. The background emission of

the cocoon and secondary rings at lower z positions, are relatively faint.

Some of the better morphological examples, showing a close correspondence to the features in Hercules A, from the $M = 50$ simulations are shown in Figures 4-6. Although approximately 3% – 10% of frames are qualitatively similar to the multi-ringed morphology of Hercules A, the brightness contrast is too great. Where there appears a prominent ring, it is usually a lone product of a hot-spot's temporary disruption, and there are no other features of comparable brightness.

Simulations with lower Mach number produce a multiple ring morphology typically with a lower brightness contrast than for higher Mach numbers. In the $M = 5$ simulations (e.g. Figures 7-9) there are abundant instances of morphologies resembling the western lobe of Hercules A: multiple rings of comparable brightness, separated appreciably along the length of the jet. The rings occurring furthest behind the head of the jet often appear in proximity to diamond shocks in the jet. Approximately 7%–15% of the $M = 5$ images are qualitatively similar to Hercules A.

In the $M = 2$ simulations (Figures 10-11) the rings have a brightness contrast relative to the cocoon that is less than or equal to the observed factor (~ 3). Compared to the hot-spots in the simulations with higher M , the brightest point on the jet axis is typically quite far to the left of the brightest rings. In $M = 2$ simulations, the cocoon and hot-spot together are dim enough that the jet itself appears prominent in comparison.

In simulations where the left boundary is closed, the turbulent eddies of the cocoon remain significant until their kinetic energy is entirely thermalised. Thus the jet is more prone to disruption in the manner described above. The outcome for an $(\eta, M) = (10^{-4}, 50)$ simulation is substantially altered, as the surging phenomenon becomes significant and frequent enough that the jet is pinched off potentially anywhere along its length. The simulated radio brightness contrast between the fresh shock features and the cocoon background is effectively reduced because the jet deposits its energy briefly at many points widely distributed along its maximal length on the z axis. Series of multiple bright rings are appear readily due to this rapid alternation. This extreme surging has been discussed in detail in Saxton et al. (2002).

4. Discussion and Conclusions

4.1. Morphology

Our simulations show that a jet with constant fluxes of mass, momentum and energy may nonetheless vary dramatically in its morphology and extent within a jet dynamical time scale, $t_{\text{dyn}} \equiv 2r_j/c_{s,j}$. In extremely light jet simulations, e.g. with $(\eta, M) = (10^{-4}, 2)$, turbulence and dense obstructions in the backflow are sufficiently important that they can pinch and break the jet essentially anywhere along its length. The disconnected forward parts of the jet are rapidly mixed into the rest of the cocoon. A new hot-spot occurs at the new, recessed, jet terminus and this hot-spot gradually burrows forward through the cocoon until it reaches the forward working surface of the lobe once more. In the transitions of these extreme surging events, arrays of ring-like shocks, derived from the disconnected jet plasma, often exceed in brightness the hot-spots and diamond shocks within the jet. This is our explanation for the rings of enhanced radio intensity in the western lobe of Hercules A.

The surging jet dynamics revealed in simulations puts the western radio emitting structures into a new perspective. If we overlook the distraction of the rings and outer parts of the western radio lobe, the innermost “shell” identified in Mason et al. (1988) and Morrison & Sadun (1996) actually resembles a hot-spot in a traditional FR2 radio source. This is located at approximately 46% of the distance from the nucleus to the outer edge of the lobe. We therefore suggest that this *is* the present western hot-spot, and that the larger, outer western radio lobe is the product of an earlier stage when the jet was not disrupted and reached out to a larger distance.

The apparent absence of hot-spots near the outer edges of the radio lobes of Hercules A is a distinctive feature reproduced in many instants in all of our simulations. However, this phenomenon is most dramatic at $M = 2$. Moreover, the occurrence of recessed hot-spots in the $M = 2$ simulations is greatest for $\eta = 10^{-4}$. The probability of an $(\eta, M) = (10^{-4}, 2)$ jet showing a jet terminus located at less than 50% of the distance to the outer edge of the lobe, is approximately 0.4.

The differences between the $M = 2$ and $M \geq 5$ simulations probably lies in the effective entrainment of matter at lower Mach numbers that is reflected in the higher rate of growth of unstable modes for low M . The minor dependence on $M \geq 5$ of the cumulative distribution functions shown in Figure 2 may be due to the increasingly vigorous nature of turbulent eddies in the cocoon. For these Mach numbers, as well, the lower η jets are more prone to disruption.

The notion of a low Mach number in Hercules A is also consistent with the morphology

of the *eastern* jet, since both jets presumably have similar properties when they emerge from the nucleus. However, inherent instabilities may cause differences of appearance at any particular moment on arcminute scales. The long “helical” portion of the eastern jet (Figure 1) has the appearance of a jet that has become unstable, that is possibly decelerating to a transonic velocity and, as a result, becoming turbulent. The transition of a relativistic jet to turbulent transonic flow occurs when $\rho_j c^2 \sim 4p$ (Bicknell 1995), which implies $\eta = \eta_{\text{crit}} \approx 4kT/\mu m_p c^2 \sim 10^{-4}$. For jets that have not made the transition to turbulent flow, $\eta < \eta_{\text{crit}}$. If the eastern jet is indeed transonic at the base of the eastern lobe, then both jets may emerge from the galaxy with a low Mach number, perhaps $2 \lesssim M \lesssim 5$. Since the western jet does not appear to have become fully turbulent, $\eta < 10^{-4}$ confirming our preference for parameters for the Western jets that involve both a low Mach number and density ratio.

The brightness asymmetry of the prominent outer ring in the western lobe is an important characteristic that is reproduced in many bright shocked rings appearing in our simulations. This effect occurs because some shock-rings are ribbon-like, i.e. flat in cross-section, with the rings tilted in the $r - z$ plane. If the greater length of the cross-section is not exactly parallel to the z axis then one side of the ring presents the observer with a wider projected area than the opposite side, at a particular orientation. The side with the narrower projected area is more extended along the line of sight, and therefore appears brighter than the side that is viewed at a less grazing angle. Therefore simple orientation effects are sufficient to explain the ring morphology of Hercules A, without resort to radical departures from axisymmetry. Nor is it necessary to consider the possibilities of directed Doppler boosting of emission from shocked plasma moving at highly relativistic velocities within the cocoon (c.f. discussion of the hot-spot of Pictor A in Saxton et al. 2002).

The relative sizes of the rings also naturally occurs as a result of the flow dynamics described here. As Figures 4-11 show, ring shocks appear with different relative sizes in different instances. In particular, the smallest “ring” in the observations corresponds to the structure surrounding a recessed hot-spot.

4.2. Radio brightness contrast

The high-resolution radio intensity maps of Hercules A (Dreher & Feigelson 1984; Gizani et al. 2002) indicate that the brightest parts of the rings are on the order of $\sim 2 - 5$ times the intensity of the radio lobe background. The flatter radio spectra of the rings indicates that they are indeed shock features like those that we have modeled in simulations. Note however, that the ring spectra are not as flat as what we expect from shocked plasma. This

may indicate that they are relatively long-lived structures (in terms of synchrotron time-scales) and this is also consistent with the rings lasting longer in the lower Mach number simulations. However, assessment of this possibility must await the publication of more detailed surface brightness and spectral index observations.

If the bright part of the ring is the thinnest projected area of the underlying ribbon-like annular shock, then by inspection, the outer ring has a thickness $\gtrsim 0.08$ times the diameter of the radio lobe in that vicinity. The surface brightness enhancement of the ring over the lobe ~ 2.5 ; hence the volumetric emissivities of material in average conditions within the ring and within the lobe generally has a ratio $j_{\nu, \text{ring}}/j_{\nu, \text{lobe}} \lesssim 31$. This contrast suggests shocks of a certain strength, since $j_{\nu} \propto \varphi p^{(3+\alpha)/2}$ where α is the radio spectral index. The shock pressure increases by a factor $\sim M^2$. This implies that the Mach number of the ring shocks is ~ 3 . Our simulations with $M = 2, 5$ are the best matches for this strength of shocks in the cocoon. This conclusion is constrained by the assumptions of the emissivity model (see § 2); however it is probably indicative.

Inspection of the synthetic radio images shows that in cases with $M = 10$ or $M = 50$, the contrast between the rings and the cocoon is typically much greater than the observationally required value ~ 3 . Many of the morphologically selected instances from the $M = 2$ and $M = 5$ simulations show the appropriate contrast. For each choice of M , the densest jets, $\eta = 10^{-2}$ produce more frames showing excessive contrast in the shock features near the terminus of the jet, relative to the secondary rings. Cases with $\eta = 10^{-4}$ give the more frames with the desired contrast relationship between rings, and we expect this to be so for a real jet that is lighter than the parameter regime our calculations could attain, $\eta \ll 10^{-4}$. Thus, on this basis, the simulations reinforce the suggestion that the jets of Hercules A are very light and have Mach number in the range $2 \lesssim M \lesssim 5$.

4.3. Orientation of Hercules A

The spherical shell models of Mason et al. (1988) and Morrison & Sadun (1996) imply geometric constraints on the orientation of the trail of shells. Assuming that such a model is correct, the shells probably are not in physical contact, otherwise their spherical form and brightness distribution would be affected greatly. If consecutive shells of radius r_n and r_{n+1} do not intersect in three dimensions, and yet are partially superimposed in projection on the sky, then they are aligned on a line at an inclination θ , which is constrained by the inequality

$$\sin \theta < \frac{\Delta z'_{n,n+1}}{r_n + r_{n+1}} \quad (1)$$

where $\Delta z'_{n,n+1} = z'_{n+1} - z'_n$ is the separation of the shell origins projected onto the plane of the sky. For Hercules A, the constraints are $\theta < 46^\circ, 47^\circ, 23^\circ$ for the pairs of visually overlapping rings as shown in the Figures 2(a) and 3(a) of Morrison & Sadun (1996).

However in our model, the luminous radio-emitting rings may in principle be separated by distances much less than their radii, and larger values of θ are feasible. On the other hand, our model explains the non-circularity of the rings, implying that $\sin \theta \approx b'/a'$ where a' and b' are the semimajor and semiminor axes of the elliptical projection of a circular ring onto the plane of the sky. Apart from the innermost bright feature which we re-identify as a buried hot-spot, we distinguish three rings clearly in the radio images, from east to west: a partially filled ellipse, one dimmer partial elliptical arc and then the bright half-ring. By measuring these features from the observations we fit ellipses and infer an inclination $\theta \approx 45^\circ \pm 10^\circ$.

4.4. Implications for the cluster environment

The two temperatures of diffuse X-ray emission from the cluster medium surrounding Hercules A may reflect the different states of gas upstream and downstream of the bow shock driven by the outer radio lobes. The observed temperature ratio is $1.7 \lesssim T/T_0 \lesssim 2.1$, which is comparable to the temperature ratios of the shocked thermal gas in some of our simulations. In Table 2 we show temperature ratios found at the point of the bow shock, and on the sides of the bow shock parallel to the jet axis. The tabulated temperature ratios indicate a lower Mach number ~ 5 , if this explanation for the two-temperature structure of the local cluster medium is correct. The temperature ratios are too small (≈ 1) for the $M = 2$ simulations.

4.5. Closing remarks

The ring structures in the western radio lobe of Hercules A are well explained as shocks in the jet cocoon, with a ribbon-like, approximately annular geometry. The absence of a strong hot-spot at the extremity of the radio lobe may be attributed to the surging of the head of the jet on length scales of $\sim 10^2$ kpc, as a result of the dynamics of the turbulent and entraining backflows in the radio lobe. The lack of a hot-spot near the edge of the lobe, the low contrast of the radio rings and the appearance of the Eastern jet all suggest a low Mach number $M \sim 2 - 5$, low density ratio $\eta < 10^{-4}$ jet. In order that the jet power be consistent with the luminosity of the source, η may be as low as 10^{-6} and this is consistent with our

view of radio galaxy jets as being composed of relativistic plasma. Our view of this radio source implied by the appearance of *both* sides is that the source is balanced on the edge of a transition to full turbulence. It is noteworthy that this may be occurring in a source which is so much more powerful than the transition FR 1/FR 2 sources and at present we can only speculate that this is related to the merger apparent in the optical observations of Hercules A (Minkowski 1957; Sadun & Hayes 1993). We have estimated an orientation such that the eastern jet makes an acute angle to the line of sight, $30^\circ \lesssim \theta < 70^\circ$, consistent with the value $\theta \approx 50^\circ$ determined from radio depolarisation measurements of Gizani & Leahy (1999). Finally we should comment on the relevance of two-dimensional simulations. These are justified *a priori* on the basis of observed ring-like structure and the simulations seem to capture a lot of the physics that is relevant to the observations. Nevertheless, it would be desirable to carry out three-dimensional simulations and test some of the features of the present work. For example, how much of a perturbation from axi-symmetry is allowable before the ring structure is destroyed and how sensitive is the Mach number dependence of the entrainment effects to the dimensionality of the simulations?

Acknowledgments

This work was supported by an Australian Research Council Large Grant, A69905341 and grants of computing time from the ANU Supercomputer Facility. We are grateful to Drs N. Gizani, M. Garrett and P. Leahy for permission to publish their radio image (Figure 1).

REFERENCES

Allington-Smith, J. R., Ellis, R., Zirbel, E. L., & Oemler, A. J. 1993, ApJ, 404, 521

Bicknell, G. V. 1995, ApJS, 101, 29

Bicknell, G. V., Dopita, M. A., Tsvetanov, Z. I., & Sutherland, R. S. 1998, ApJ, 495, 680

Blondin, J. M. & Lukfin, E. A. 1993, ApJS, 88, 589

Carvalho, J. C. & O'Dea, C. P. 2001, ApJS, accepted, —

Colella, P. & Woodward, P. R. 1984, J. Comput. Phys., 54, 174

Conner, S. R., et al. 1998, AJ, 115, 37

Dreher, J. W. & Feigelson, E. D. 1984, Nature, 308, 43

Fanaroff, B. L. & Riley, J. M. 1974, MNRAS, 167, 31P

Garrington, S. T, Leahy, J. P., Conway, R. G., & Laing, R. A. 1988, Nature, 331, 147

Gizani, N. A. B., Garrett, M. A., & Leahy, J. P. 2002, PASA, 19, 69

Gizani, N. A. B. & Leahy, J. P. 1999, New Astronomy Review, 43, 639

Greenstein, J. L. 1962, ApJ, 135, 679

Laing, R. A. 1988, Nature, 331, 149

Mason, A., Morrison, P., & Sadun, A. C. 1988, Nature, 333, 640

Minkowski, R. 1957, in IAU Symp. 4: Radio astronomy, Volume 4 107

Morrison, P. & Sadun, A. 1996, MNRAS, 278, 265

Owen, F. N. & Laing, R. A. 1989, MNRAS, 238, 357

Perley, R. A., Bridle, A. H., Willis, A. G., & Fomalont, E. B. 1980, AJ, 85, 499

Rosen, A., Hughes, P. A., Duncan, G. C., & Hardee, P. E. 1999, ApJ, 516, 729

Sadun, A. C. & Hayes, J. J. E. 1993, PASP, 105, 379

Saxton, C. J., Sutherland, R. S., Bicknell, G. V., Blanchet, G. F., & Wagner, S. J. 2002, A&A, submitted, –

Siebert, J., Kawai, N., & Brinkmann, W. 1999, A&A, 350, 25

Trussoni, E., Feretti, L., Massaglia, S., & Parma, P. 2001, A&A, 366, 788

van Breugel, W. & Fomalont, E. B. 1984, ApJ, 282, L55

Yates, M. G., Miller, L., & Peacock, J. A. 1989, MNRAS, 240, 129

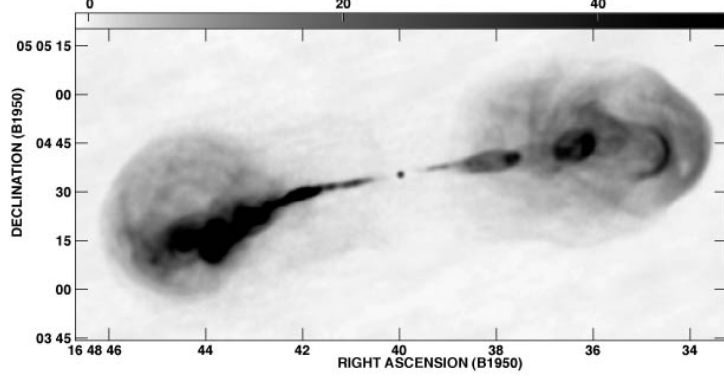


Fig. 1.— Radio image (at 18 cm) of Hercules A, its lobes, jets and associated rings, from Gizani et al. (2002) and published with the permission of those authors.

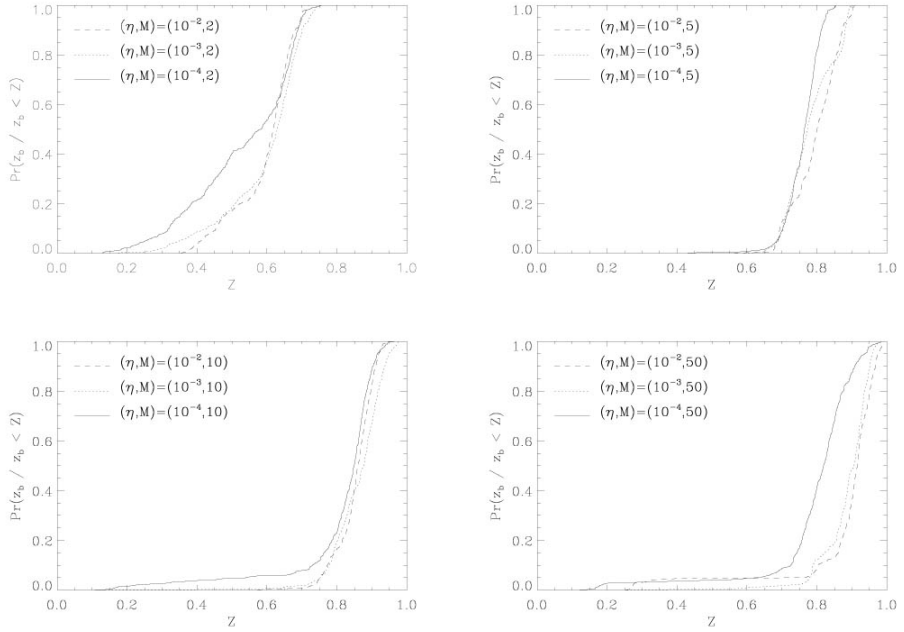


Fig. 2.— Cumulative distribution functions expressing the frequency and extent of surging in terms of ratios of the z positions of the bow shock and jet head. The jet's head position z_h is defined as the forwardmost cell where the jet plasma remains unmixed with external gas, i.e. $\varphi = 1$. We show cases with $M = 2, 5, 10, 50$. These are simulations with an open left boundary, and $\eta = 10^{-2}, 10^{-3}, 10^{-4}$ for dashed, dotted and solid lines respectively.

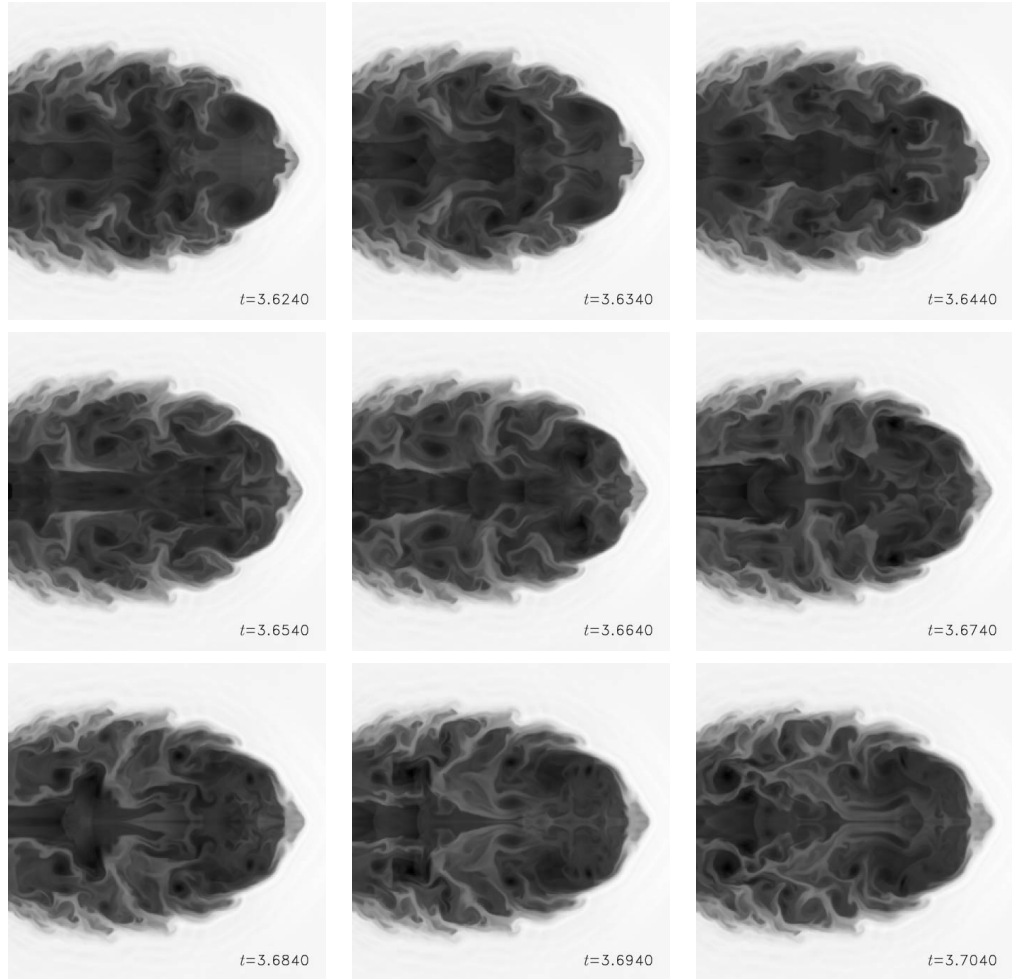


Fig. 3.— A sequences of $\log \rho$ cross-sections of the jet showing as it is affected by dense fingers of external gas entrained into the cocoon.

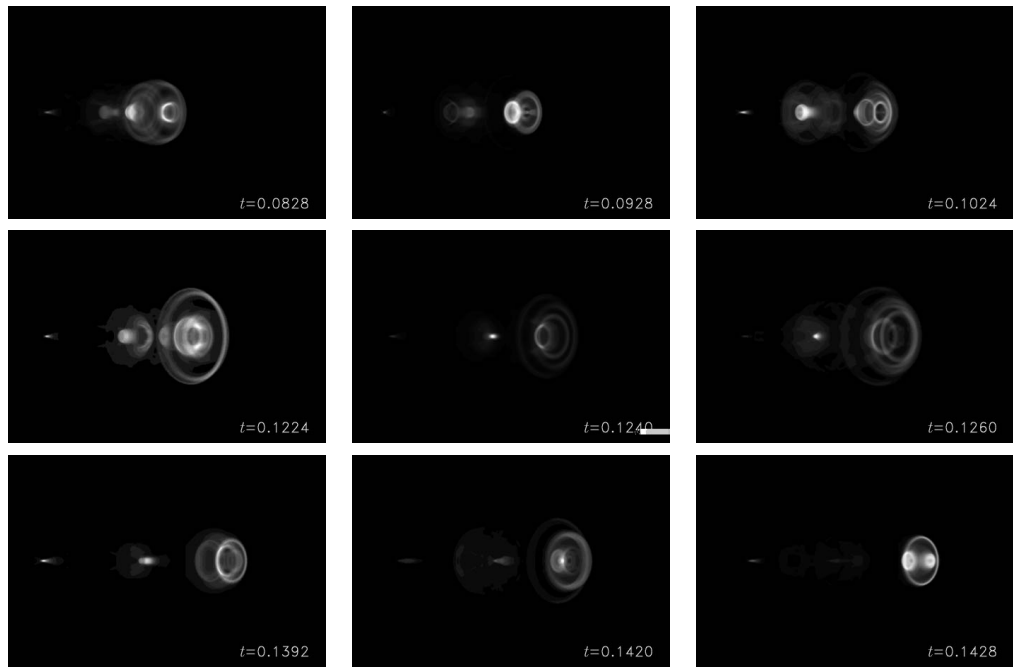


Fig. 4.— Selected images rendered with the jet at an orientation of $\theta = 45^\circ$ to the line of sight, from the simulation with jet parameters $(\eta, M) = (10^{-4}, 50)$ and an open left boundary.

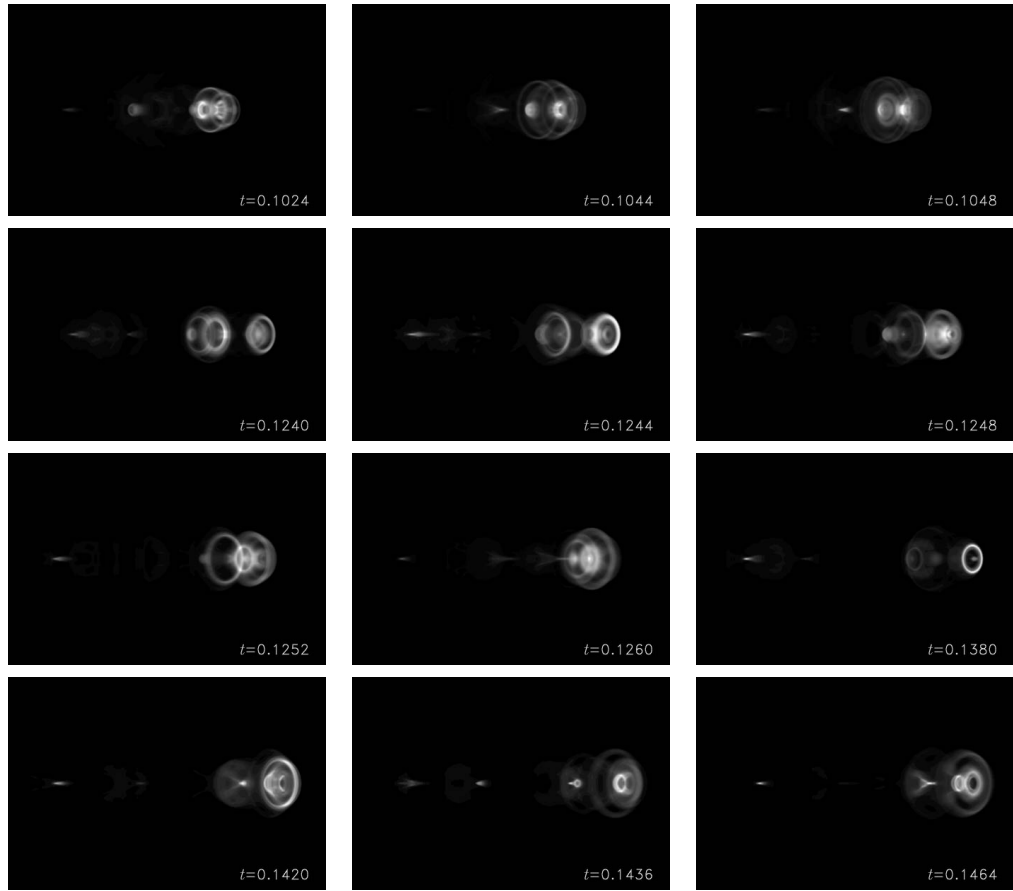


Fig. 5.— Selected images rendered with the jet at an orientation of $\theta = 45^\circ$ to the line of sight, from the simulation with jet parameters $(\eta, M) = (10^{-3}, 50)$ and an open left boundary.

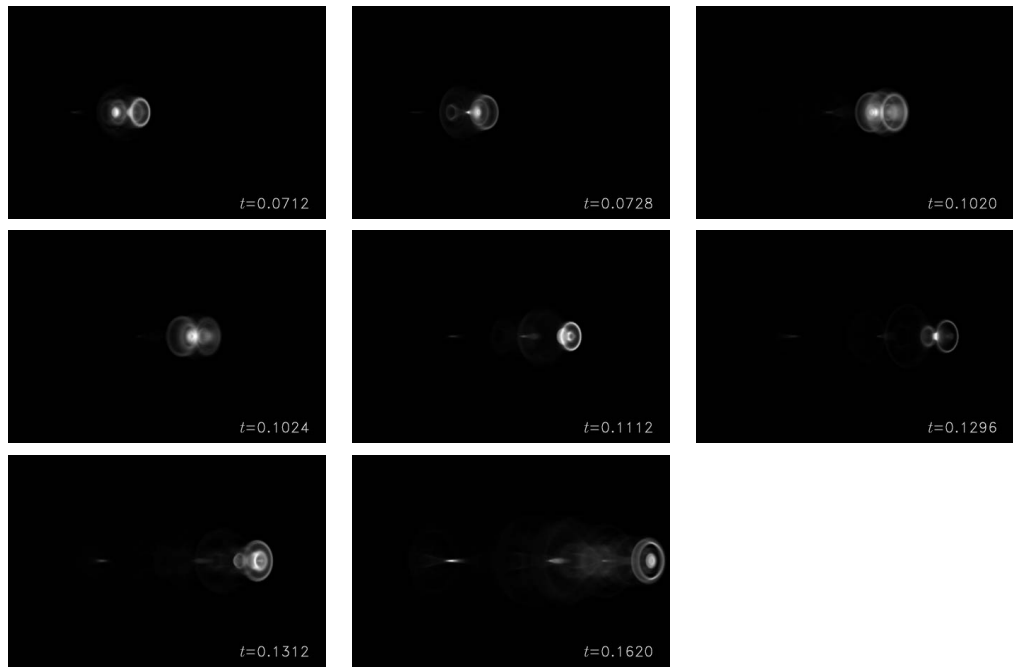


Fig. 6.— Selected images rendered with the jet at an orientation of $\theta = 45^\circ$ to the line of sight, from the simulation with jet parameters $(\eta, M) = (10^{-2}, 50)$ and an open left boundary.

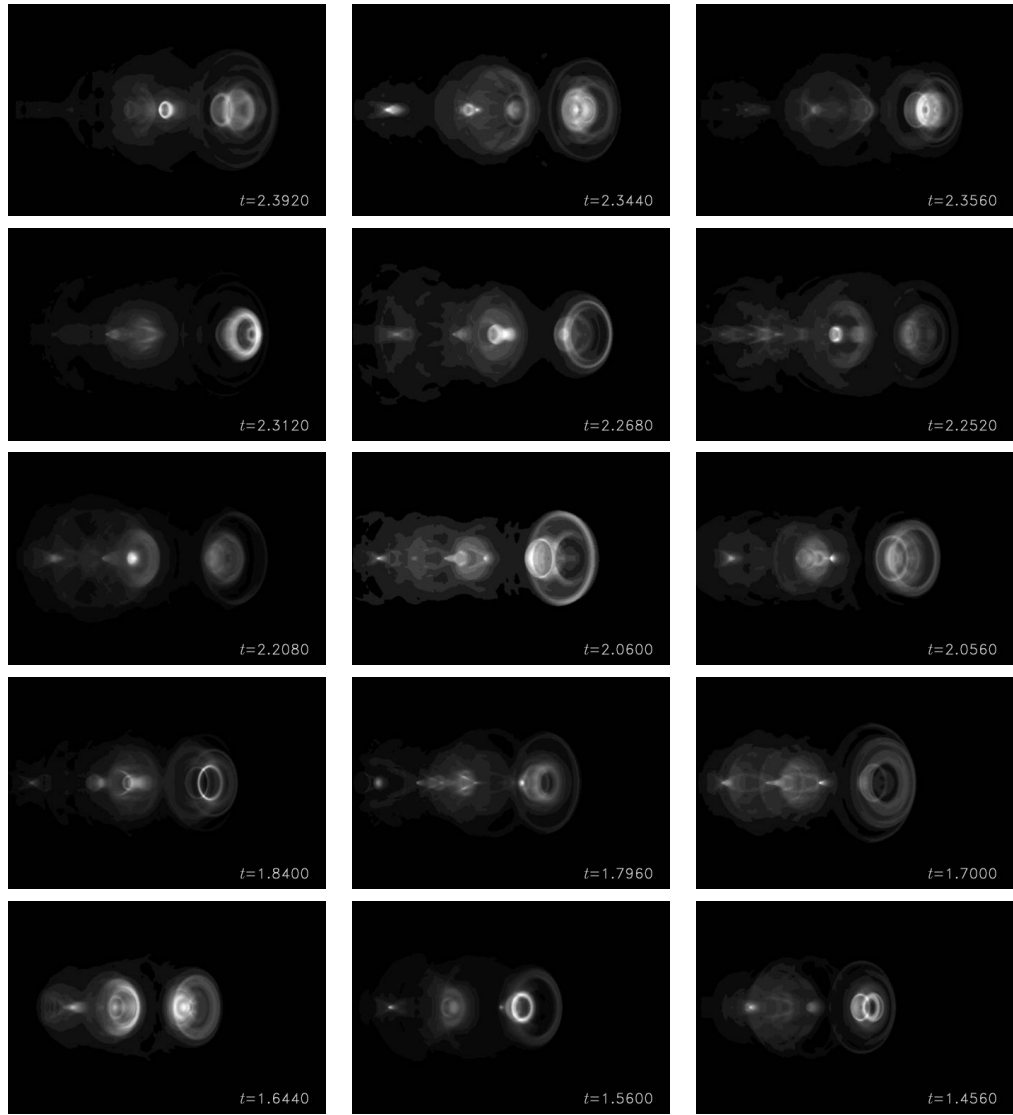


Fig. 7.— Selected images rendered with the jet at an orientation of $\theta = 45^\circ$ to the line of sight, from the simulation with jet parameters $(\eta, M) = (10^{-4}, 5)$ and an open left boundary.

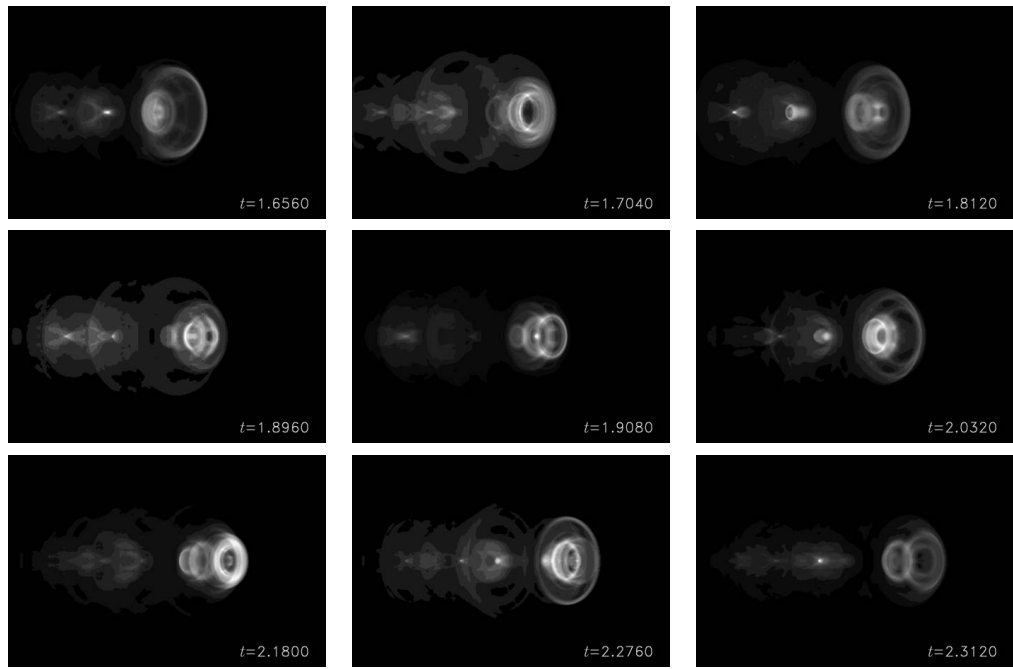


Fig. 8.— Selected images rendered with the jet at an orientation of $\theta = 45^\circ$ to the line of sight, from the simulation with jet parameters $(\eta, M) = (10^{-3}, 5)$ and an open left boundary.

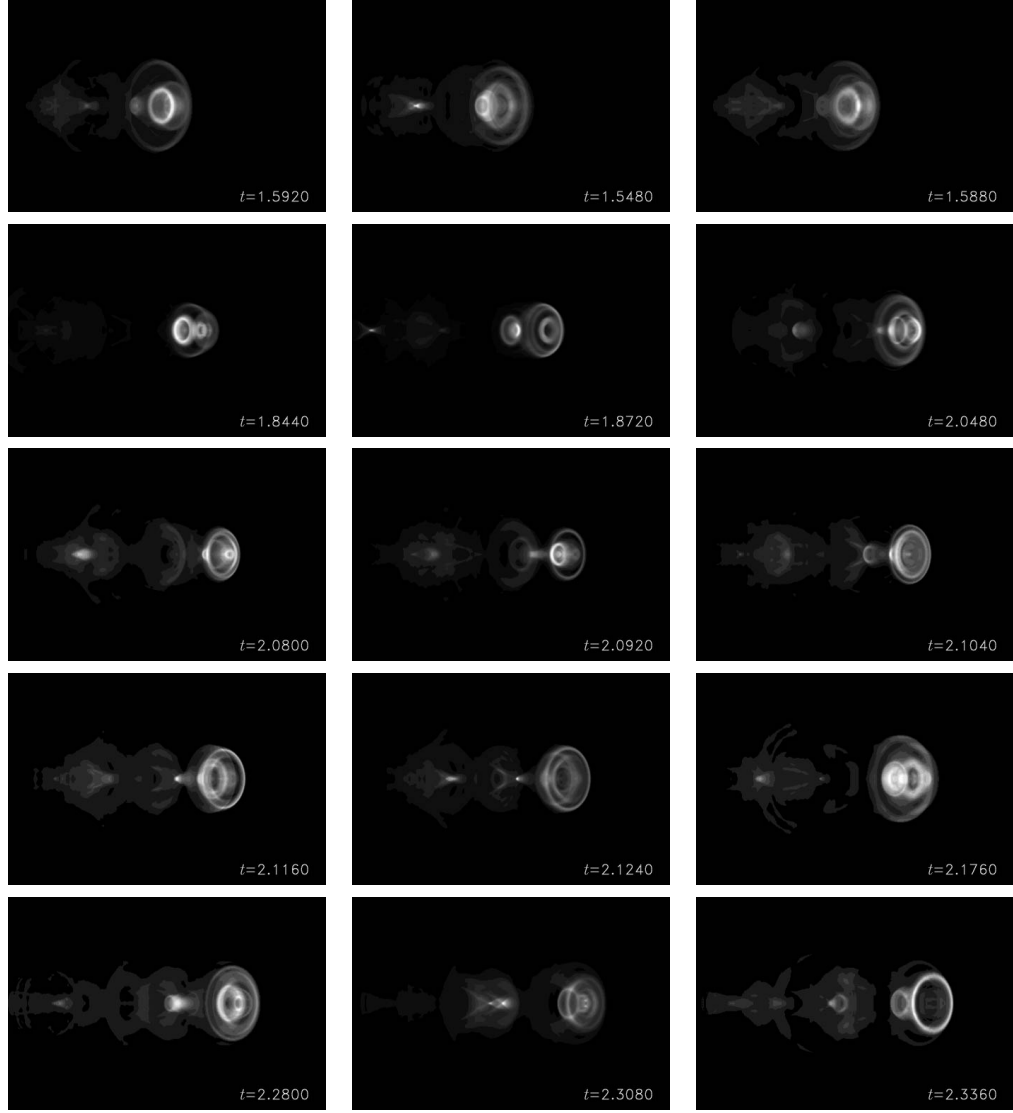


Fig. 9.— Selected images rendered with the jet at an orientation of $\theta = 45^\circ$ to the line of sight, from the simulation with jet parameters $(\eta, M) = (10^{-2}, 5)$ and an open left boundary.

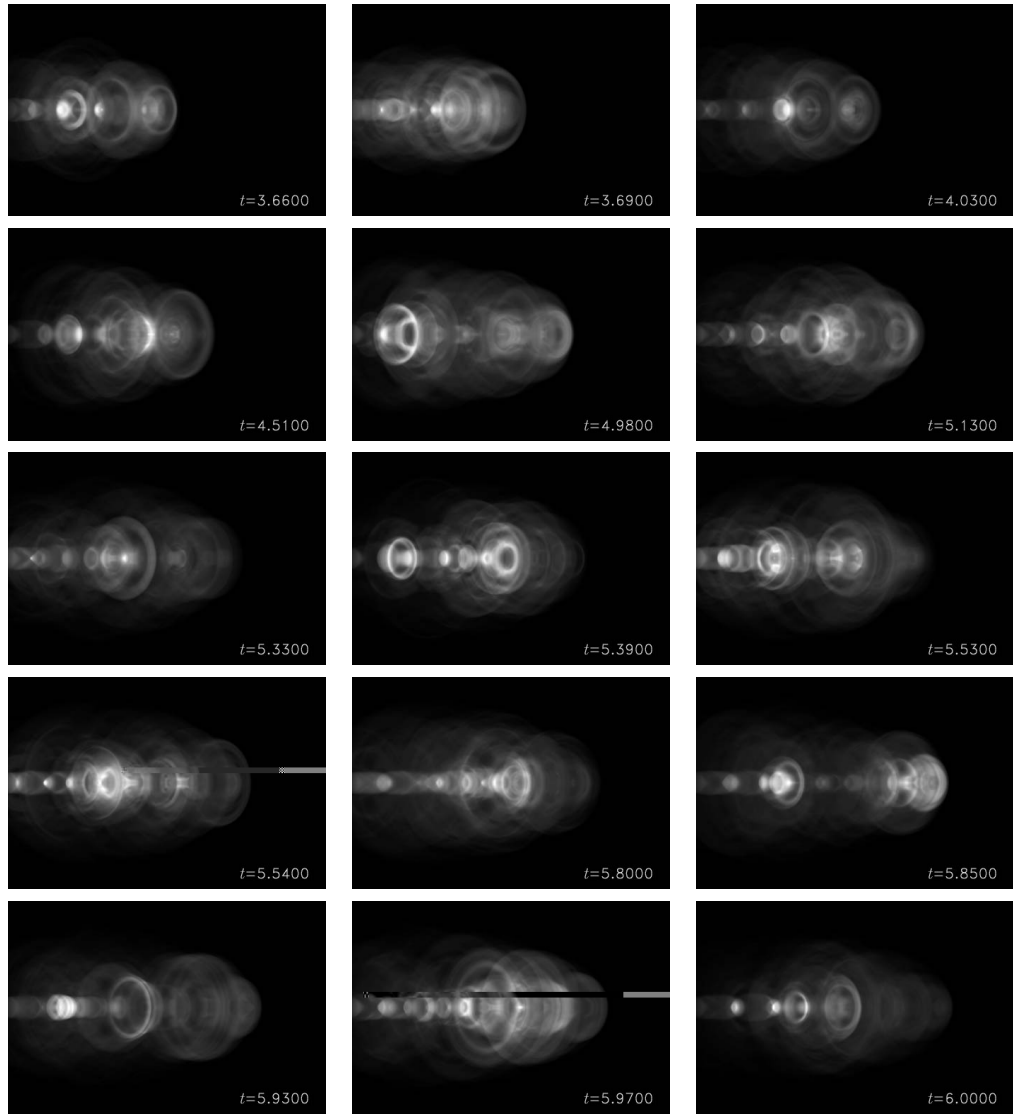


Fig. 10.— Selected images rendered with the jet at an orientation of $\theta = 45^\circ$, from the simulation with jet parameters $(\eta, M) = (10^{-4}, 2)$ and an open left boundary.

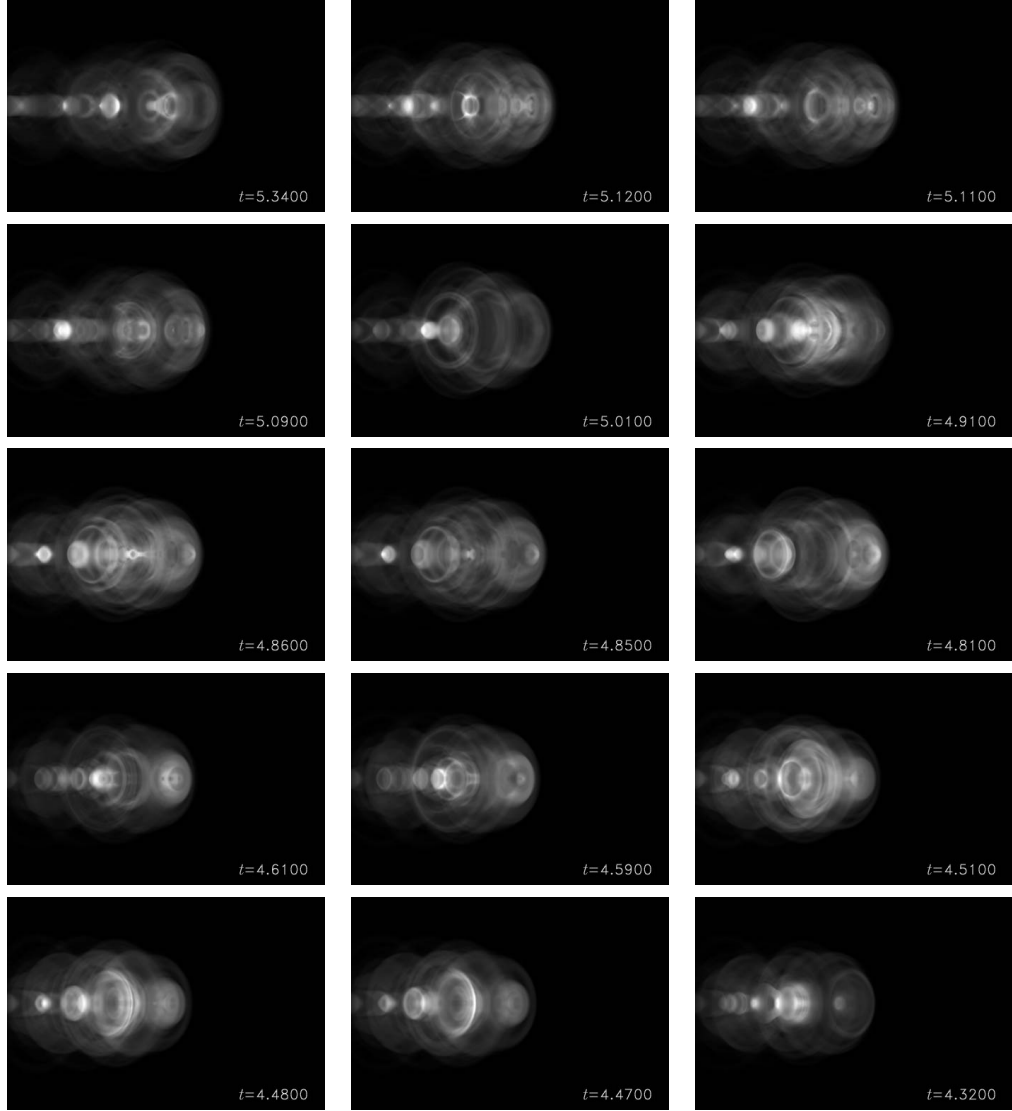


Fig. 11.— Selected images rendered with the jet at an orientation of $\theta = 45^\circ$, from the simulation with jet parameters $(\eta, M) = (10^{-2}, 2)$ and an open left boundary.

Table 1: Classical evaluations of the velocity, mass flux, force and power of a jet with radius $r_j = 0.54/h$ kpc for our choices of the parameters (η, M) . These are non-relativistic evaluations, assuming cosmic abundances, an electron number density of $n_0 = 7.8 \times 10^{-3}$ cm $^{-3}$ and a temperature of $kT_0 = 2.45$ keV in the undisturbed ambient medium.

η	M	$\frac{v_j}{(T/T_0)^{1/2}}$ (cm . s $^{-1}$)	$\frac{\dot{M}_j}{(n/n_0)(T/T_0)^{1/2}}$ (M_\odot . yr $^{-1}$)	$\frac{F_j}{(n/n_0)(T/T_0)}$ (dyn)	$\frac{L_j}{(n/n_0)(T/T_0)^{3/2}}$ (erg . s $^{-1}$)
10^{-2}	2	1.59×10^9	3.61×10^{-2}	4.16×10^{33}	5.03×10^{42}
10^{-3}	2	5.03×10^9	1.14×10^{-2}	4.16×10^{33}	1.59×10^{42}
10^{-4}	2	1.59×10^{10}	3.61×10^{-3}	4.16×10^{33}	5.03×10^{43}
10^{-2}	5	3.97×10^9	9.02×10^{-2}	2.31×10^{34}	5.03×10^{43}
10^{-3}	5	1.26×10^{10}	2.85×10^{-2}	2.31×10^{34}	1.59×10^{44}
10^{-4}	5	3.97×10^{10}	9.02×10^{-3}	2.31×10^{34}	5.03×10^{44}
10^{-2}	10	7.95×10^9	1.80×10^{-1}	1.66×10^{35}	3.70×10^{44}
10^{-3}	10	2.51×10^{10}	5.71×10^{-2}	1.66×10^{35}	1.17×10^{45}
10^{-4}	10	7.95×10^{10}	1.80×10^{-2}	1.66×10^{35}	3.70×10^{45}
10^{-2}	50	3.97×10^{10}	9.02×10^{-1}	2.26×10^{36}	4.49×10^{46}
10^{-3}	50	1.26×10^{10}	2.85×10^{-1}	2.26×10^{36}	1.42×10^{47}
10^{-4}	50	3.97×10^{11}	9.02×10^{-2}	2.26×10^{36}	4.49×10^{47}

Table 2: Typical temperatures in shocked thermal gas at the front of the bow shock (T_b/T_0) and on the flank where the shock is approximately parallel to the jet (T_f/T_0), for various choices of the system parameters.

η	M	T_b/T_0	T_f/T_0	η	M	T_b/T_0	T_f/T_0
10^{-2}	2	1.08	1.02	10^{-2}	10	3.28	1.54
10^{-3}	2	1.08	1.02	10^{-3}	10	3.64	1.76
10^{-4}	2	1.11	1.03	10^{-4}	10	2.97	1.45
10^{-2}	5	1.71	1.18	10^{-2}	50	20.6	4.45
10^{-3}	5	1.63	1.13	10^{-3}	50	27.1	6.53
10^{-4}	5	1.69	1.17	10^{-4}	50	13.9	6.71